Nano Energy (▮▮▮▮) ▮, ▮▮▮–▮▮▮

Available online at www.sciencedirect.com

ScienceDirect

journal homepage: www.elsevier.com/locate/nanoenergy

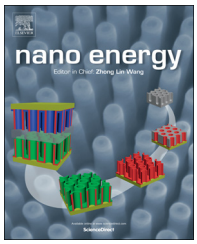


RAPID COMMUNICATION

# Unraveling film transformations and device performance of planar perovskite solar cells

Tze-Bin Song[a,b], Qi Chen[a,b], Huanping Zhou[a,b], Song Luo[a,b], Yang (Michael) Yang[a,b], Jingbi You[a,b], Yang Yang[a,b,*]

[a]Department of Materials Science and Engineering, University of California Los Angeles, Los Angeles, CA 90095, USA
[b]California NanoSystems Institute, University of California Los Angeles, Los Angeles, CA 90095, USA

Received 17 December 2014; received in revised form 12 January 2015; accepted 12 January 2015

KEYWORDS
Perovskite;
Photovoltaic;
Transformation;
Secondary phase;
Decomposition

**Abstract**
High performance (>15%) organometaltrihalide based solar cells have been demonstrated in recent years to be a promising candidate for low cost photovoltaics and have attracted significant attention in the photovoltaic community. Planar thin film perovskite solar cells, which are more easily fabricated, provide a great platform to investigate the perovskite film properties. Until now, many of the properties of perovskite thin films remain unexplored and the link between film properties and device performances is in need of investigation to further boost the efficiencies of these devices. Here, film transformation of perovskite materials is demonstrated as a critical factor to reach high performance in planar heterojunction $CH_3NH_3PbI_{3-x}Cl_x$ solar cells. Reaction induced secondary phases can be observed and carefully controlled by tuning the processing conditions during film formation. The properties of $CH_3NH_3PbI_{3-x}Cl_x$ films are investigated and a possible formation pathway is proposed. It is shown that the high performance devices are attainable with a small portion of secondary phases coexisting with $CH_3NH_3PbI_3$ film and power conversion efficiencies of up to 14% are achieved. The correlations between the phases present, device performance and physical properties are discussed to identify the role of the secondary phases in $CH_3NH_3PbI_{3-x}Cl_x$ material.


## 1. Introduction

Thin film solar cells, such as $CuInGaSe_2$ (CIGS), CdTe, $Cu_2ZnSnSe_2$ (CZTS) and amorphous Si (a-Si) have been developed as promising alternatives to crystalline silicon

*Corresponding author at: Department of Materials Science and Engineering, University of California Los Angeles, Los Angeles, CA 90095, USA.
*E-mail address:* yangy@ucla.edu (Y. Yang).

http://dx.doi.org/10.1016/j.nanoen.2015.01.025
2211-2855/

solar cells as more cost-effective technologie [1-6]. As a result of the efficient direct band gap absorption, the thickness of thin film solar cells could be effectively reduced to sub-micrometer or even hundreds of nanometer The potential low cost (cents/watt) of solar cells can be achieved through the combination of reduced material cost and high device performance [7]. The high performance of CIGS and other compound absorbers, however, relies on vacuum based and/or high temperature processes which would lead to high manufacturing costs and limit the choice of substrates. In recent years, hybrid organic/inorganic perovskite absorbers, especially methylammonium lead halide $CH_3NH_3PbX_3$ (X=Cl, Br and I)-based, have attracted significant attention as promising materials for thin film solar cells. Extraordinary power conversion efficiencies (PCEs) of over 17% were achieved during the past five years and the materials have been demonstrated as capable of being prepared using a number of low temperature processes, making these materials especially attractive for low cost and scalable manufacturing of next generation thin film photovoltaic devices [8-11].

Perovskite $CH_3NH_3PbX_3$-based solar cells have shown to possess desirable properties such as an extremely high absorption coefficient, efficient ambipolar transport, and a tunable direct band gap, allowing them to be excellent solar absorbers and carrier transporters [12-18]. However, how to effectively control the material growth, film formation, and film quality is still under investigation. In previous works, the morphology, stoichiometry and crystallinity of these materials were found to affect the device performance significantly [19-22]. Deposition techniques, treatments and film formation conditions are critical to achieve high efficiency solar cells [23-25]. Dualeh et al. showed that the depositing a $CH_3NH_3PbI_{3-x}Cl_x$ precursor onto mesoporous titanium dioxide ($TiO_2$) structure under proper annealing temperature can lead to formation of $CH_3NH_3PbI_3$ perovskite material resulting in reduced pin holes within the film [19]. Eperson et al. demonstrated that the annealing temperature, film thickness and thickness of compact $TiO_2$ layer can influence the coverage of $CH_3NH_3PbI_{3-x}Cl_x$ which would further impact the device performance [20]. These studies furthered our understanding on the correlation between film formation and device performance. However, to further improve the device performance, it is crucial to understand the film's properties and the quality of the films from the perspective of phase formation. During the formation of $CH_3NH_3PbX_3$ perovskite film from the molecular solution, different phases are observed and those phases coexisting with the $CH_3NH_3PbI_3$ phase in the films are considered secondary phases. Secondary phases play a crucial role in the semiconductor materials and could significantly alter the device performance. For example, the order vacancy compound (OVC) $CuIn_3Se_5$ phase in CIGS improves electrical transport within the n-type cadmium sulfide (CdS) layer [26-28]. On the other hand, the semimetallic phase $Cu_2Se$ in CZTS could lead to the formation of shunt paths and recombination centers and thus deteriorating the device performance [29]. In this paper, the phase transition during the $CH_3NH_3PbI_{3-x}Cl_x$ film formation was observed and the secondary phases' effects on the film formation, film properties and device performance were investigated.

## 2. Experimental section

### 2.1. Material preparation

$CH_3NH_3I$ (MAI) was synthesized by reacting 24 ml of methylamine (33 wt% in absolute ethanol, Sigma) with 10 ml of hydroiodic acid (HI) (57 wt% in water, Aldrich) in a round-bottom flask at 0 °C for 2 h with stirring. The precipitation was extracted by putting the solution on a rotary evaporator and carefully removing the solvent at 50 °C. The raw product $CH_3NH_3I$ was re-dissolved in absolute ethanol and precipitated upon the addition of diethyl ether. After filtration, the step was subsequently repeated. The solid was collected and dried at 60 °C in a vacuum oven for 24 h. The $PbCl_2$, Li-bis(trifluoromethanesulfonyl) imide (Li-TFSI) and tert-butylpyridine (tBP) were purchased from Aldrich. Spiro-OMeTAD was purchased from Lumtec.

### 2.2. Device fabrication

Low temperature $TiO_2$ solution was prepared as previous report [30]. The $TiO_2$ solution (3 mg/ml) was spin-coated on pre-cleaned ITO substrates at 3000 rpm. and then baked 150 °C for 30 min. A 0.73 M perovskite solution was prepared from $PbCl_2$ and MAI with (1:3 mole ratio) in DMF and spin-coated onto the ITO/$TiO_2$ substrate at 2000 rpm. and then baked at 100 °C for different times inside a dry air glovebox under 25 ppm $H_2O$. The Spiro-OMeTAD was used as a hole transporting layer and dissolved in chlorobenzene (180 mg/ml). The Li-TFSI was dissolved in acetonitrile (170 mg/ml) and 20 μl tBP. The Li-TFSI solution was added to the Spiro-OMeTAD solution at a ratio of 1:40. Then, Li salt doped Spiro-OMeTAD solution was spin-coated at 2000 rpm. onto the perovskite layer. Finally, a gold electrode was evaporated onto the hole transport layer. The device area was defined with shadow mask with an area of 0.114 $cm^2$ for measurement.

### 2.3. Instruments and characterizations

X-ray diffration (XRD) data were collected on Panalytical X'Pert Pro X-ray Powder Diffractometer with Cu Kα radiation ($\lambda$=1.54056 Å). Scanning electron microscopy (SEM) were performed with field-emission electrons using Nova 230 Nano SEM. Time-resolved photoluminescence (TR-PL) using Picoharp single counting system using 632.8 nm semiconductor laser with a pulse width less than 0.2 ns and with repetition rate of 1 MHz as excitation source was used for carrier lifetime measurement. The photovoltaic performance was characterized without any encapsulation under an AM1.5G filter at 100 mW/$cm^2$ in air using Newport Oriel 92192 Solar Simulator and the intensity was calibrated using a certified silicon photodiode.

## 3. Results and discussion

The $CH_3NH_3PbI_{3-x}Cl_x$ perovskite absorber was deposited using a one-step method onto the tin doped indium oxide (ITO)/$TiO_2$ substrates by spin coating from a 1:3 molar ratio solution of $PbCl_2$ and $CH_3NH_3I$ (MAI) in dimethyl foramide (DMF) and

Please cite this article as: T.-B. Song, et al., Unraveling film transformations and device performance of planar perovskite solar cells, Nano Energy (2015), http://dx.doi.org/10.1016/j.nanoen.2015.01.025

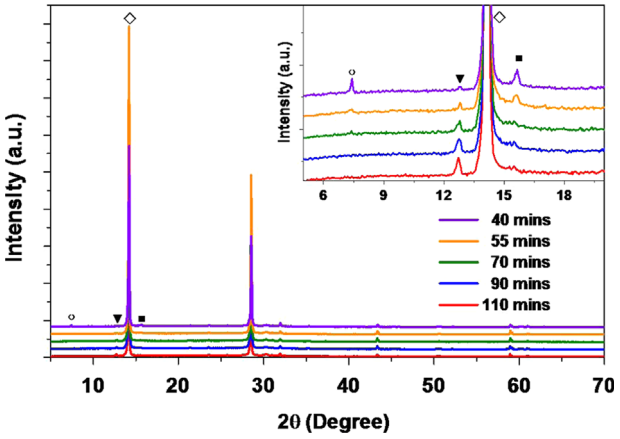


**Fig. 1** X-ray diffraction (XRD) patterns of $CH_3NH_3PbI_{3-x}Cl_x$ film formation. The phase transformation was observed from annealing times of 40 min to 110 mins. The inset is the enlarged XRD result within 5-20°.

annealed at 100 °C, which is reported to promote good film coverage and can provide sufficient energy for the perovskite phase formation (Details of the film preparation are shown in experimental section) [19]. The $CH_3NH_3PbI_3$ is most commonly prepared by thermal annealing at 80∼100 °C. Annealing temperatures below this range (between 60 and 80 °C) would result in slow transformation rates, while temperatures lower than 60 °C could be too low to drive the transformation. Higher annealing temperatures (>120 °C) would accelerate the decomposition of $CH_3NH_3PbI_3$ and induce a poor film coverage [19,20]. Thus, the temperature was fixed at 100 °C to investigate the phase transformation at different annealing times. The phase transformation was characterized by x-ray diffraction (XRD) with results shown in Fig. 1. The peak at $2\theta$=7.4 degrees arises from the precursor complex and those of $2\theta$=12.7°, 14.2° and 15.6° corresponds to $PbI_2$ (0 0 1), $CH_3NH_3PbI_3$ (1 1 0) and $CH_3NH_3PbCl_3$ (1 0 0) orientation respectively (used as signature peaks for tracking phase transformation and indicated by circle, triangle, diamond and square in Fig. 1). All observed peaks came from the aforementioned four phases and no extra phases were present according to the observation of the diffraction patterns. As seen in the XRD measurement, the precursor complex phase almost disappeared at 70 min annealing time which indicated the nearly complete transformation from precursor to solid phases. Surprisingly a certain amount of $PbI_2$phase was observed even at 40 min annealing, which is before the complete transformation as identified by the disappearance of the precursor complex peak at $2\theta$=7.4°. This indicated that $PbI_2$ phase formed under this annealing temperature easily even for less than 40 min (XRD pattern at 25 min annealing time shown in the Figure S1) and it was deduced to come from the ion exchange between $PbCl_2$ and MAI. The generated $PbI_2$ reacted meanwhile with MAI to form $CH_3NH_3PbI_3$, and $PbCl_2$ reacted with $CH_3NH_3Cl$ (MACl), which was generated from $PbCl_2$ and MAI, to form the $CH_3NH_3PbCl_3$ phase. The $PbI_2$ peaks are still present even with the incorporation of excess MAI into the precursor solution, as shown in Figure S2. The result indicated that the $PbI_2$ formed at an early stage and was later transformed into $CH_3NH_3PbI_3$perovskite phase by reacting with MAI. Except for$CH_3NH_3PbI_3$, other phases are hardly seen from full XRD spectrum because of the extremely small amounts of those phases. In order to evaluate the relative amount of the precursor complex, $PbI_2$ and$CH_3NH_3PbCl_3$ phase present during the phase change, the area ratio of the precursor complex peak at $2\theta$=7.4°, $PbI_2$ (0 0 1) and $CH_3NH_3PbCl_3$ (1 0 0), as relative to the $CH_3NH_3PbI_3$ (1 1 0) peak were calculated using Gaussian fitting. At 55 min annealing time, the ratio of precursor complex, $CH_3NH_3PbCl_3$ and $PbI_2$ to $CH_3NH_3PbI_3$ were 0.21%, 1.79% and 0.16% respectively. When the annealing time was increased to 70 min, the amount of the precursor complex and $CH_3NH_3PbCl_3$ phase reduced to 0.05% and 1.25% and the $PbI_2$ phase increased to 0.53%. It can be assumed that the $CH_3NH_3PbI_3$ phase formation was nearly complete and the increase in the relative amount of $PbI_2$ phase mainly came from the $CH_3NH_3PbI_3$ phase decomposition and precursor reaction. Moreover, the reaction of $PbCl_2$ with MAI to generate $PbI_2$ caused the depletion of $PbCl_2$ which in turn would facilitate the decomposition of $CH_3NH_3PbCl_3$ phase reflected by the deceasing $CH_3NH_3PbCl_3$ peak ratio. After 90 min annealing, the area ratio of the $PbI_2$ (0 0 1) peak relative to the $CH_3NH_3PbI_3$ (1 1 0) peak increased up to 1.70%. The films with longer annealing time, for example 110 min, generated more $PbI_2$ phase and less $CH_3NH_3PbCl_3$ phase. It is noted that the secondary phases will coexist in the solution processed $CH_3NH_3PbI_{3-x}Cl_x$ film and it would be a challenge to obtain a pure $CH_3NH_3PbI_3$ phase. Summarizing the information obtained from XRD characterization on the solution processed $CH_3NH_3PbI_{3-x}Cl_x$ phase transformation, possible transformation pathways are proposed in Fig. 2. Table 1.

At path (1), $PbCl_2$ and MAI in the DMF reacted to form $PbI_2$ and MACl while coexisting with MAI and a possible precursor complex. During annealing at path (2), $PbI_2$ reacts with MAI and $PbCl_2$ reacts with MACl to form $CH_3NH_3PbI_3$and $CH_3NH_3PbCl_3$. The $CH_3NH_3PbI_3$ phase formed from path (2) can decompose under thermal annealing at 100 °C to generate $PbI_2$ phase, $CH_3NH_2$ and HI at path (3). The excess MAI can continue to react with $PbCl_2$ to generate $PbI_2$, facilitating the decomposition of the $CH_3NH_3PbCl_3$phase (4). When the excess MAI depleted, the decomposition mechanism of $CH_3NH_3PbI_3$ and $CH_3NH_3PbCl_3$ phases dominates, and the relative amount of $PbI_2$ phase rose gradually. This proposed pathway takes into account both results from the XRD characterization here and previous reports [19,31,32].

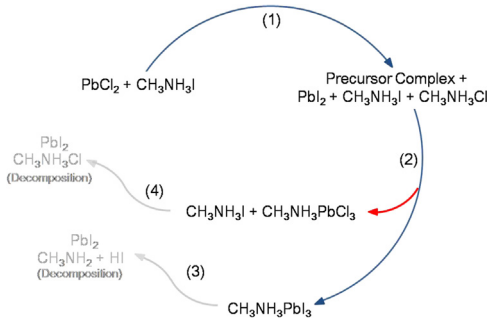


**Fig. 2** Possible transformation pathway of solution processed $CH_3NH_3PbI_{3-x}Cl_x$ film: (1) $PbCl_2+3CH_3NH_3I \rightarrow PbI_2+CH_3NH_3I+2CH_3NH_3Cl$; (2) $PbI_2+CH_3NH_3I \rightarrow CH_3NH_3PbI_3$; $PbCl_2+CH_3NH_3Cl \rightarrow CH_3NH_3PbCl_3$; (3) $CH_3NH_3PbI_3 \rightarrow PbI_2+CH_3NH_2+HI$; (4) $CH_3NH_3PbCl_3+3CH_3NH_3I \rightarrow (1)+CH_3NH_3Cl$.

Please cite this article as: T.-B. Song, et al., Unraveling film transformations and device performance of planar perovskite solar cells, Nano Energy (2015), http://dx.doi.org/10.1016/j.nanoen.2015.01.025

**Table 1** The averaged four device parameters of $V_{OC}$, $J_{SC}$, FF, and Eff with varying annealing time.

| | $V_{OC}$(V) | $J_{SC}$ (mA/cm$^2$) | FF (%) | Eff (%) |
|---|---|---|---|---|
| 40 min | 0.978 | 19.35 | 68.94 | 13.04 |
| 55 min | 1.018 | 19.64 | 70.04 | 14.00 |
| 70 min | 1.033 | 19.37 | 70.37 | 14.08 |
| 90 min | 1.038 | 18.82 | 71.15 | 13.89 |
| 110 min | 1.024 | 18.15 | 69.15 | 12.85 |

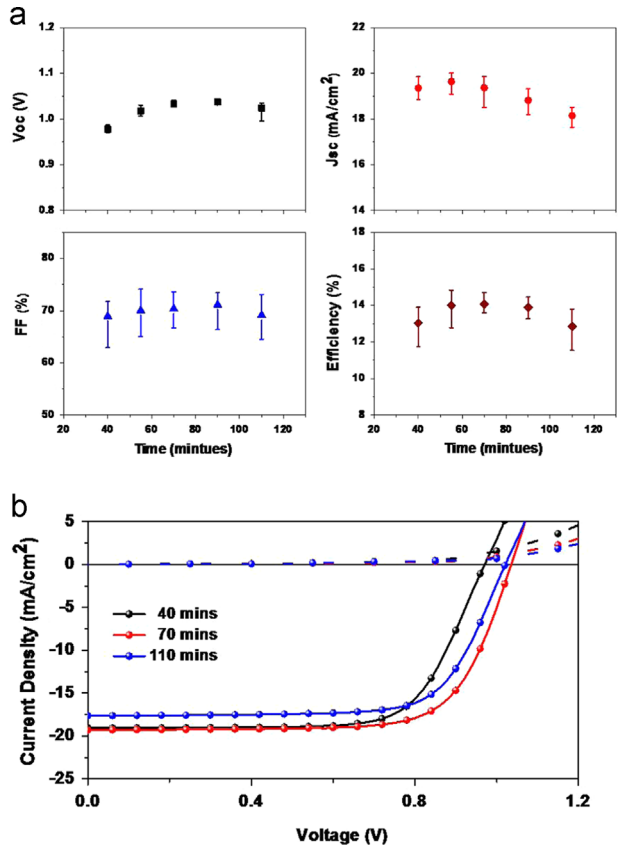


**Fig. 3** Device performance of the $CH_3NH_3PbI_{3-x}Cl_x$ films with varying annealing times (a) the summarized device parameters. (b) Typical current density-voltage characteristics for 40 min, 70 min and 110 min annealing time.

The effects of these secondary phases present in $CH_3NH_3PbI_3$ film were characterized based on device performance, film morphologies and carrier lifetime tests. $CH_3NH_3PbI_3$ films with different annealing conditions were prepared, while lithium slat doped Spiro-OMeTAD was employed as the hole transport layer and finally gold (Au) was evaporated as the back electrode. Current density-voltage (*J*-*V*) curves were measured by reverse bias scan under 1 sun AM 1.5G illumination and device parameters are shown in Fig. 3a. Typical *J*-*V* curves for the three conditions are shown in Fig. 3b, where the perovskite film were obtained from 40, 70 and 110 min annealing, corresponding to the early formation, near completed and the over-annealing stages. The highest averaged PCE was achieved for the perovskite film annealed for 70 min and it corresponds to the near completed stage where the smallest amount of secondary phases is present (less than 2% for the sum of the four specific peak areas corresponding to the four phases). At annealing times shorter or longer than 70 min, the device performances were reduced. From the summarized device parameters chart in Fig. 3a, perovskite films with 40 min annealing time exhibited poor open circuit voltage ($V_{OC}$) and slightly lower fill factor (FF).When increasing the annealing time to 55 min, the $V_{OC}$ and FF were improved by 4% and 1.5% respectively. During this period, the total amount of the secondary phases was reduced from 4.3% to 2.1%. In addition to the decrease in the amount of the precursor complex and $CH_3NH_3PbCl_3$ phase, the gradual increase of $PbI_2$ phase in the film at 70 min annealing together attributed to an improved $V_{OC}$ and FF, but a slightly lower short circuit current ($J_{SC}$). The $PbI_2$ phase was reported to improve the device performance by passivating the grain boundaries which generally worked as recombination centers [32,33]. However, excessive $PbI_2$ phase will reduce the light absorption efficiency in the film due to the larger band gap of $PbI_2$ (2.4 eV) which contributed to the lower $J_{SC}$ [19]. After 90 min of annealing, the percentage of the secondary phases present in the film rose to 4.0% mainly due to an increase of $PbI_2$ phase. The $V_{OC}$ of the devices were higher in comparison to that of annealing for 40 min where a similar amount of secondary phases was present, although with different compositions (more precursor phase and less $PbI_2$). Thus the precursor phase could be the main reason behind the lower $V_{OC}$ of the device at 40 min annealing time. The PCEs of those devices with over 90 min annealing are still low, however, mainly limited by the low $J_{SC}$ value (Device performance after 190 min of annealing is shown in Figure S3). While the devices obtained from perovskite film with 70 min of annealing exhibited high average PCEs, those with 55 min of annealing exhibited the highest averaged $J_{SC}$ among all the conditions. Therefore controlling the $PbI_2$ phase within 0.5% the amount of $CH_3NH_3PbI_3$ and tuning the amounts of precursor and $CH_3NH_3PbCl_3$ phases in the perovskite films are important to simultaneously achieve efficient light absorption, effective grain boundary passivation and reduced recombination centers.

Furthermore, the $CH_3NH_3PbI_{3-x}Cl_x$ film morphologies during the transformation were characterized by scanning electron microscopy (SEM) as shown in Fig. 4. A high surface coverage (>95%) of $CH_3NH_3PbI_{3-x}Cl_x$ films were achieved with thermal annealing at 100 °C within 70 min of annealing which reduced the possibility of shunt paths formation thereby reducing leakage current in the solar cells. The high surface coverage obtained within 70 min of annealing in this study indicates that surface coverage was not a major factor for the changes in device performance instead the evolution of the secondary phases played a vital role in device performance. When the annealing time exceeds 70 min, bright spots and voids between grain boundaries appeared, which were deduced to be coming from the decomposition of $CH_3NH_3PbI_3$ phase into $PbI_2$ phase and the loss of $CH_3NH_3PbCl_3$ phase. At annealing times of 110 min or longer, the surface coverage gradually decreased and the original conformal films were broken into small grains and branches (SEM images with different scales shown in Figure S4) and more pronounced void formation was observed

Please cite this article as: T.-B. Song, et al., Unraveling film transformations and device performance of planar perovskite solar cells, Nano Energy (2015), http://dx.doi.org/10.1016/j.nanoen.2015.01.025

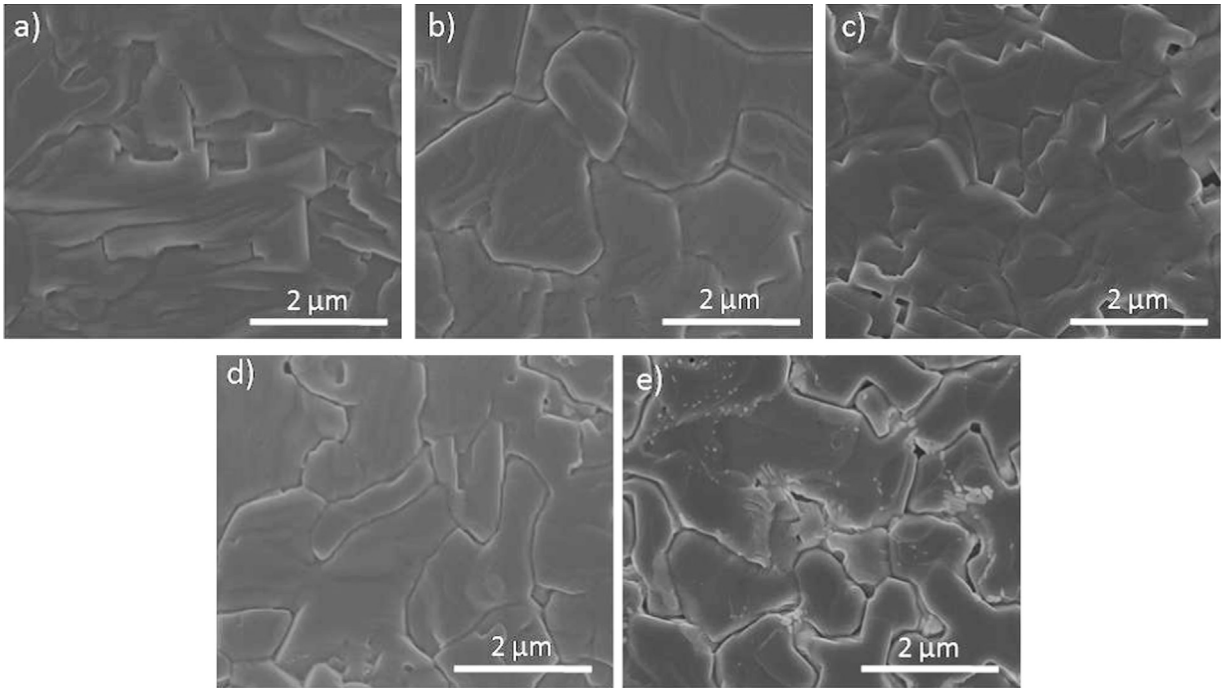


**Fig. 4** SEM images of perovskite film morphologies annealing at 100 °C for (a) 40 min (b) 55 min (c) 70 min (d) 90 min and (e) 110 min.

between the crystal grains. Such changes in the microstructure may lead to direct contact between the electron and hole transporting layers, leading to an increase in the leakage current of the devices was increased due to these shunt paths formation. In addition, an increase in voids indicates a less effective absorption area within the absorber. Thus, a decrease in device performance was attributed to the combined effects of changes in the amount of $PbI_2$ phase and changes in the thin film morphology at longer annealing times.

Time-resolved photoluminescence (TRPL) measurements with a 632 nm wavelength and 1 MHz frequency pulsed laser were performed on $TiO_2/CH_3NH_3PbI_{3-x}Cl_x$ films to best simulate the device structure at room temperature and the results are shown in Fig. 5 measuring the peak emission at 775 nm. The TR-PL data was fitted by two exponential decay curves and the minority carrier lifetime ($\tau$) of the films obtained at different conditions were 0.44 μs, 0.89 μs and 0.53 μs corresponding to annealing times of 40 min, 70 min and 110 min respectively. Longer minority carrier lifetime is associated with longer diffusion length ($L_D = \sqrt{D\tau}$), $D$ is the diffusion coefficient of carriers and reduced carrier recombination rates. For films annealed for less than 70 min, the precursor phase and other secondary phases can act as recombination centers in the material or induce stronger interface recombination with the hole transport layer or electron transport layer which would cause the $V_{OC}$ to drop significantly. It is interesting to note that the shorter carrier lifetime did not influence the $J_{SC}$ in the device performance, e.g. the absorber obtained at 40 min. This is the first time to our knowledge that this effect is observed in the $CH_3NH_3PbI_{3-x}Cl_x$ perovskite solar cells. The $J_{SC}$ reflects the collection efficiency of the p-i-n junction relative to the total number of carriers generated by light absorption. Comparing the 40 min and 70 min annealed films, the total amount of generated charges does not vary significantly possibly because

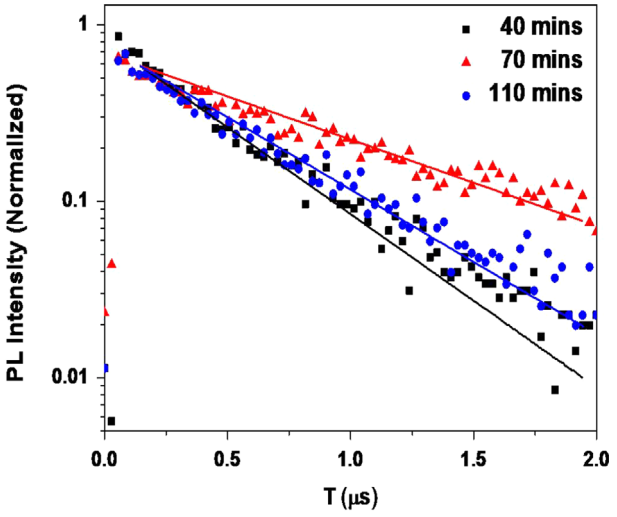


**Fig. 5** Time-resolved photoluminescence of perovskite film with (a) 40 min (b)70 min (c) 110 min on $TiO_2$ substrates at room temperature.

most of the $CH_3NH_3PbI_3$ phase was formed by 40 min and the electrical field across the perovskite layer can sweep the photogenerated carriers rapidly even with the presence of secondary phases. When the films were annealed at longer times (>110 min), the $PbI_2$ phase became the dominant secondary phase in the films and the perovskite gains were segmented according to SEM characterization. The shorter $\tau$ can be directly correlated with the decrease in $V_{OC}$ of the device performance which in turn is due to the increase of secondary phases and extent of carrier recombination. Compared with the previous studies based on vapor-assisted solution process (VASP) of $CH_3NH_3PbI_3$ perovskite solar cells, Chen et al.

Please cite this article as: T.-B. Song, et al., Unraveling film transformations and device performance of planar perovskite solar cells, Nano Energy (2015), http://dx.doi.org/10.1016/j.nanoen.2015.01.025

showed that over a certain amount of $PbI_2$ formation caused the minority carrier lifetime slightly decreased. Moreover, it did not change the film morphologies significantly [33]. However, in the one-step solution processed $CH_3NH_3PbI_{3-x}Cl_x$, the phase transformation resulted in different film morphologies and the consequently varying device performances. Moreover, the TR-PL results correspond with previous reports using impedance spectroscopic measurement that showed short electron lifetime resulted from incomplete reaction between $PbI_2$ and MAX, and from excessive $PbI_2$ formation in mesoporous structured $CH_3NH_3PbI_{3-x}Cl_x$ solar cells [19] The effects on minority carrier lifetime and morphologies are in good agreement with the current-voltage characteristic of the devices and those films with proper annealing time (55–70 min) exhibited decent minority carrier lifetime ($>0.8$ μs) and film coverage.

## 4. Conclusions

In this paper, the evolution of various phases was shown through a series of characterizations for the phase transformation of perovskite thin films based on solution processed $CH_3NH_3PbI_{3-x}Cl_x$. XRD results indicated that multiple secondary phases, including a precursor complex, $PbI_2$, and $CH_3NH_3PbCl_3$ formed during the perovskite formation. The device performance showed that less secondary phases will result in better PCEs, while it is a challenge to achieve pure $CH_3NH_3PbI_3$ phase from the single step co-deposition process from $PbCl_2$ and MAI precursors. The SEM and TR-PL results were consistent with the device performance measurements and further elucidated the relation between phase transformation and device performance. Based on these results, possible reaction pathways were proposed to unravel the evolution of phases as the film formation occurred during the annealing process. The phase transformation based on different film preparation processes, e.g. two step solution process, vacuum deposition, and co-deposition solution process from $PbI_2$ precursor instead of $PbCl_2$ should be further studied to address the Cl species effect and to improve device performance. We believe that the present understanding of the phases' effects will facilitate the rational design of perovskite materials and expedite the development of this emerging photovoltaic technology.

## Acknowledgments

The authors gratefully acknowledge the financial support from Air Force Office of Scientific Research (Grant number: FA9550-12-1-0074, Program Manager Dr. Charles Lee).

## Appendix A. Supporting information

Supplementary data associated with this article can be found in the online version at http://dx.doi.org/10.1016/j.nanoen.2015.01.025.

## References

[1] A.G. Aberle, Thin Solid Films 517 (2009) 4706–4710.
[2] T.T. Chow, Appl. Energy 87 (2010) 365–379.
[3] A. Chirilă, S. Buecheler, F. Pianezzi, P. Bloesch, C. Gretener, A.R. Uhl, C. Fella, L. Kranz, J. Perrenoud, S. Seyrling, R. Verma, S. Nishiwaki, Y.E. Romanyuk, G. Bilger, A. N. Tiwari, Nat. Mater. 10 (2011) 857–861.
[4] W. Wang, M.T. Winkler, O. Gunawan, T. Gokmen, T.K. Todorov, Y. Zhu, D.B. Mitzi, Adv. Energy Mater. 4 (2014) 1301465.
[5] M. Gloeckler, I. Sankin, Z. Zhao, IEEE J. Photovolt 3 (2013) 1389–1393.
[6] A. Polizzotti, I.L. Repins, R. Noufi, S.-H. Wei, D.B. Mitzi, Energy Environ. Sci. 6 (2013) 3171–3182.
[7] J. Peng, L. Lu, H. Yang, Renew. Sust. Energ. Rev. 19 (2013) 255–274.
[8] H. Zhou, Q. Chen, G. Li, S. Luo, T.-B. Song, H.-S. Duan, Z. Hong, J. You, Y. Liu, Y. Yang, Science 345 (2014) 542–546.
[9] N.J. Jeon, J.H. Noh, Y.C. Kim, W.S. Yang, S. Ryu, S.I. Seok, Nat. Mater. 13 (2014) 897–903.
[10] J. You, Z. Hong, Y. Yang, Q. Chen, M. Cai, T.-B. Song, C.-C. Chen, S. Lu, Y. Liu, H. Zhou, Y. Yang, ACS Nano 8 (2014) 1674–1680.
[11] P. Docampo, J.M. Ball, M. Darwich, G.E. Eperon, H.J. Snaith, Nat. Commun. 4 (2013) 2761.
[12] J. Even, L. Pedesseau, C. Katan, J. Phys. Chem. C 118 (2014) 11566–11572.
[13] J.-H.Y. Li Lang, H.-R. Liu, H.J. Xiang, X.G. Gong, Phys. Lett. A 378 (2014) 290–293.
[14] M.M. Lee, J. Teuscher, T. Miyasaka, T.N. Murakami, H.J. Snaith, Science 338 (2012) 643–647.
[15] G. Xing, N. Mathews, S. Sun, S.S. Lim, Y.M. Lam, M. Grätzel, S. Mhaisalkar, T.C. Sum, Science 342 (2013) 344–347.
[16] J.H. Noh, S.H. Im, J.H. Heo, T.N. Mandal, S.I. Seok, Nano Lett. 13 (2013) 1764–1769.
[17] G.E. Eperon, S.D. Stranks, C. Menelaou, M.B. Johnston, L. Herz, H. Snaith, Energy Environ. Sci. 7 (2014) 982–988.
[18] S.A. Kulkarni, T. Baikie, P.P. Boix, N. Yantara, N. Mathews, S.G. Mhaisalkar, J. Mater. Chem. A 2 (2014) 9221–9225.
[19] A. Dualeh, N. Tétreault, T. Moehl, P. Gao, M.K. Nazeeruddin, M. Grätzel, Adv. Funct. Mater. 24 (2014) 3250–3258.
[20] G.E. Eperon, V.M. Burlakov, P. Docampo, A. Goriely, H.J. Snaith, Adv. Funct. Mater. 24 (2013) 151–157.
[21] Q. Wang, Q. Dong, Z. Xiao, Y. Yuan, J. Huang, Energy Environ. Sci. 7 (2014) 2359–2365.
[22] B.-W. Park, B. Philippe, T. Gustafsson, K. Sveinbjörnsson, A. Hagfeldt, E.M.J. Johansson, G. Boschloo, Chem. Mater. 26 (2014) 4466–4471.
[23] Q. Chen, H. Zhou, Z. Hong, S. Luo, H.-S. Duan, H.-H. Wang, Y. Liu, G. Li, Y. Yang, J. Am. Chem. Soc. 136 (2013) 622–625.
[24] P.-W. Liang, C.-Y. Liao, C.-C. Chueh, F. Zuo, S.T. Williams, X.-K. Xin, J. Lin, A.K.Y. Jen, Adv. Mater. 26 (2014) 3748–3754.
[25] Z. Xiao, C. Bi, Y. Shao, Q. Dong, Q. Wang, Y. Yuan, C. Wang, Y. Gao, J. Huang, Energy Environ. Sci. 7 (2014) 2619–2623.
[26] D. Schmid, M. Ruckh, F. Grunwald, H.W. Schock, J. Appl. Phys. 73 (1993) 2902–2909.
[27] M. Bär, S. Nishiwaki, L. Weinhardt, S. Pookpanratana, O. Fuchs, M. Blum, W. Yang, J.D. Denlinger, W.N. Shafarman, C. Heske, Appl. Phys. Lett. 93 (2008) 244103.
[28] H. Peng, C. Xie, D.T. Schoen, K. McIlwrath, X.F. Zhang, Y. Cui, Nano Lett. 7 (2007) 3734–3738.
[29] A. Fairbrother, E. García-Hemme, V. Izquierdo-Roca, X. Fontané, F.A. Pulgarín-Agudelo, O. Vigil-Galán, A. Pérez-Rodríguez, E. Saucedo, J. Am. Chem. Soc. 134 (2012) 8018–8021.
[30] K. Wojciechowski, M. Saliba, T. Leijtens, A. Abate, H. Snaith, Energy Environ. Sci. 7 (2014) 1142–1147.
[31] A. Dualeh, P. Gao, S.I. Seok, M.K. Nazeeruddin, M. Grätzel, Chem. Mater. 26 (2014) 6160–6164.
[32] T. Supasai, N. Rujisamphan, K. Ullrich, A. Chemseddine, T. Dittrich, Appl. Phys. Lett. 103 (2013) 183906.

Please cite this article as: T.-B. Song, et al., Unraveling film transformations and device performance of planar perovskite solar cells, Nano Energy (2015), http://dx.doi.org/10.1016/j.nanoen.2015.01.025

[33] Q. Chen, H. Zhou, T.-B. Song, S. Luo, Z. Hong, H.-S. Duan, L. Dou, Y. Liu, Y. Yang, Nano Lett. 14 (2014) 4158–4163.

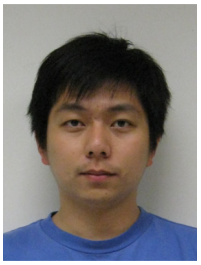

**Tze-Bin Song** is a Ph.D. candidate at the University of California Los Angeles (UCLA), in Materials Science and Engineering under the supervision of Prof. Yang Yang. He received his B.S. degree from National Tsing-Hua University, Taiwan, in 2007 and M.S. degree from University of Florida in 2010, both in Materials Science and Engineering. His research interests include development of thin film solar cells, transparent electrodes and material/device characterizations. During his Ph.D. studies, he had an internship in International Business Machines, T. J. Watson, NY, where he participated in developing the advanced integration technique.

**Dr. Qi Chen** received his Ph.D degree in Materials Science and Engineering from University of California at Los Angeles (UCLA) in the year 2012. Now, he is working as a postdoc fellow in California Nanosystem Institute (CNSI) of UCLA. And his research focuses on hybrids materials, polymer blends for various applications, such as Photovoltaics, sensors, detectors etc.

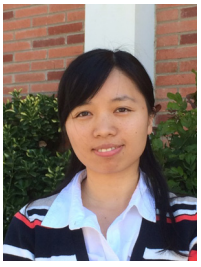

**Dr. Huanping Zhou** received her Ph.D degree in Inorganic Chemistry from Peking University in the year 2010. Now, she is working as a postdoc fellow in Prof. Yang Yang's lab in UCLA. Her research focuses on nanomaterials, thin films and optoelectronics, etc.

**Yang (Michael) Yang** received B.E.in Electrical Engineering from Zhejiang University, China in 2009. He was a research intern between 2009 and 2010 at institute of Chemistry, Chinese Academy of Sciences (ICCAS), under the supervision of Prof. Yongfang Li. He is now a PhD Candidate in Prof. Yang Yang's group, in the Department of Materials Science and Engineering at UCLA. His research interests include organic and organic-inorganic hybrid optoelectronic device and their spectroscope study.

**Dr. Jingbi You** is a postdoctoral researcher in Prof. Yang Yang's lab at University of California, Los Angeles. He got his PhD from Chinese Academy of Science, Institute of Semiconductors. His research interests include organic solar cells, perovskite solar cells and plasmonics. He has published more than 40 pre-reviewed Journals.

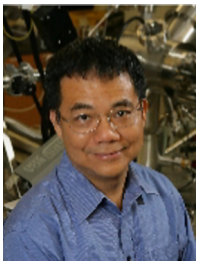

**Yang Yang** received his M.S. and Ph.D. in Physics and Applied Physics from the University of Massachusetts, Lowell in 1988 and 1992, respectively. Before he joined UCLA in 1997, he served as the research staff in UNIAX (now DuPont Display) from 1992 to 1996. Yang is now the Carol and Lawrence E. Tannas Jr Endowed Chair Professor of Materials Science at UCLA. He is also the Fellow of SPIE, RSC and the Electromagnetic (EM) Academy. He is an expertise in the fields of organic, inorganic and organic/inorganic hybrid electronics and the development and fabrication of related devices, such as photovoltaic cells, LEDs, transistor and memory devices.

Please cite this article as: T.-B. Song, et al., Unraveling film transformations and device performance of planar perovskite solar cells, Nano Energy (2015), http://dx.doi.org/10.1016/j.nanoen.2015.01.025